Molecular Therapy
Nucleic Acids
Original Article

# Effective splicing restoration of a deep-intronic *ABCA4* variant in cone photoreceptor precursor cells by CRISPR/*Sp*Cas9 approaches

Pietro De Angeli,[1] Peggy Reuter,[1] Stefan Hauser,[4,5] Ludger Schöls,[4,5] Katarina Stingl,[2,3] Bernd Wissinger,[1] and Susanne Kohl[1]

[1]Institute for Ophthalmic Research, Centre for Ophthalmology, University Hospital Tübingen, 72076 Tübingen, Germany; [2]Centre for Ophthalmology, University Hospital Tübingen, 72076 Tübingen, Germany; [3]Center for Rare Eye Diseases, University of Tübingen, 72076 Tübingen, Germany; [4]German Center for Neurodegenerative Diseases (DZNE), 72076 Tübingen, Germany; [5]Department of Neurodegenerative Diseases, Hertie-Institute for Clinical Brain Research and Center of Neurology, University of Tübingen, 72076 Tübingen, Germany

**Stargardt disease is an autosomal recessively inherited retinal disorder commonly caused by pathogenic variants in the *ABCA4* gene encoding the ATP-binding cassette subfamily A member 4 (ABCA4) protein. Several deep-intronic variants in *ABCA4* have been classified as disease causing. By strengthening a cryptic splice site, deep-intronic variant c.5197-557G>T induces the inclusion of a 188-bp intronic sequence in the mature mRNA, resulting in a premature termination codon. Here, we report the design and evaluation of three CRISPR-Cas9 approaches implementing *Streptococcus pyogenes* Cas9 (single and dual guide RNA) or *Streptococcus pyogenes* Cas9 nickase (dual guide RNA) for their potential to correct c.5197-557G>T-induced aberrant splicing in minigene splicing assays and patient-derived cone photoreceptor precursor cells. The different strategies were able to rescue correct splicing by up to 83% and increase the overall correctly spliced transcripts by 1.8-fold, demonstrating the successful CRISPR-Cas9-mediated rescue in patient-derived photoreceptor precursor cells of an *ABCA4* splicing defect. The results provide initial evidence of possible permanent splicing correction for Stargardt disease, expanding the therapeutic toolbox to counteract deep-intronic pathogenic variants in *ABCA4*.**

## INTRODUCTION

Stargardt disease (STGD1) is the most frequent juvenile hereditary macular dystrophy with an estimated prevalence of one in 8,000–10,000 people.[1] STGD1 is most commonly inherited as an autosomal recessive condition caused by variants in the *ABCA4* gene, which encodes a retina-specific ATP-binding cassette transporter involved in the shuttling of *N*-retinylidene-phosphatidylethanolamine from the intradiscal space to the cytoplasm in photoreceptors.[2] Disease-associated variants in *ABCA4* can also result in cone-rod dystrophy, fundus flavimaculatus and retinitis pigmentosa, and are one of the most common causes of inherited retinal dystrophy.[3,4] STGD1 is characterized by loss of central vision due to accumulation of toxic retinoid compounds such as *N*-retinylidene-*N*-retinylethanolamine (A2E) in retinal pigment epithelial cells, leading to degeneration and photoreceptor cells death.[1] Although a number of clinical trials (ClinicalTrials.gov: NCT03772665, ClinicalTrials.gov: NCT02402660) targeting the toxic buildup of A2E in the retina are ongoing, to date there is no treatment for STGD1.

*ABCA4* is a 128-kb large gene composed of 50 exons.[1] Following the discovery of *ABCA4* and its association with STGD1, the investigation of the mutation spectrum primarily focused on exonic point mutations, including missense and nonsense mutations, small indels, and canonical splice site variants.[5–7] Despite comprehensive genetic testing, numerous clinically diagnosed STGD1 cases remained unsolved or carried only a single heterozygous *ABCA4* variant.[7,8] In the attempt to solve cases of STGD1 missing heritability, Braun et al. reported the first evidence of deep-intronic pathogenic variants (DIVs) in *ABCA4* resulting in missplicing.[9] Since then, a considerable number of additional recurrent or unique *ABCA4* DIVs have been identified and characterized.[10,11]

Owing to their location in the non-coding sequence of a gene, DIVs represent an attractive therapeutic target in monogenic disease. DIVs often lead to the activation of a cryptic splice site or intronic splicing enhancers, resulting in the inclusion of an intronic sequence (pseudoexon) in the mature mRNA.[12,13] Such pseudoexons lead to the disruption of the open reading frame and frequently are predicted to result in a shortened protein due to the occurrence of a premature termination codon. However, the presence of a premature termination codon triggers the cellular nonsense-mediated decay (NMD) pathway, leading to the degradation of the mutant aberrant mRNA transcript.[14]

Received 21 February 2022; accepted 20 July 2022;
https://doi.org/10.1016/j.omtn.2022.07.023.

**Correspondence:** Pietro De Angeli, Institute for Ophthalmic Research, Centre for Ophthalmology, Elfriede-Aulhorn-Strasse 5–7, 72076 Tübingen, Germany.
**E-mail:** pietro.de-angeli@med.uni-tuebingen.de

Although gene augmentation therapy is an attractive strategy for recessive diseases such as STGD1, the size of the *ABCA4* gene coding sequence (~6.8 kb) exceeds the packaging capacity of adeno-associated viral vectors, the most advanced delivery system for ocular gene therapy.[15] Alternative therapeutic approaches for large genes rather focus on certain types of mutations such as splicing mutations through splicing modulation by antisense oligonucleotides (AONs) and splicing correction by CRISPR-Cas9 genome editing. While AON-mediated splicing modulation in *ABCA4* has already been explored in several studies,[12,13,16] CRISPR-Cas9-mediated splicing correction studies have not yet been reported. Moreover, therapeutics based on genome-editing technologies would possibly enable permanent splicing rescue as opposed to AON treatments, where recurrent and continuous readministration is needed.[17,18]

By means of genome-editing strategies, the deletion of deleterious DIVs and the surrounding genomic context has been shown to rescue the normal splicing of *CFTR* transcripts in cystic fibrosis and of *CEP290* in patients with Leber congenital amaurosis. The latter is currently being applied to patients affected by LCA10 in a first-in-man phase I/II clinical safety trial (ClinicalTrials.gov identifier NCT03872479).[19,20]

We aimed to test the amenability of CRISPR-Cas9-mediated rescue of DIV-induced missplicing in *ABCA4*. As a target the *ABCA4* DIV c.5197-557G>T, which induces the retention of a 188-bp pseudoexon in the mature mRNA, was selected. The c.5197-557G>T variant strengthens a cryptic splice donor site (human splicing finder matrix: REF:44.51, ALT:71.65), inducing the retention of an intronic sequence between exons 36 and 37 (Figure 1A).[21] This leads to the frameshift of the open reading frame and the formation of a premature termination codon p.(Met1733*), which is expected to result in the degradation of mutant transcripts via NMD.

Three different CRISPR-Cas9-based approaches based on *Streptococcus pyogenes* Cas9 (*Sp*Cas9) or *Sp*Cas9-nickase were designed and tested in minigene assays in HEK293T and patient-derived cone photoreceptor precursor cells (CPCs): (1) dual guide RNA/*Sp*Cas9 (dgRNAs/*Sp*Cas9) utilizing two guide RNAs (gRNAs) designed to target regions flanking the DIV; (2) gRNA/*Sp*Cas9-nickase rescue (dgRNAs/*Sp*Cas9n) based on the use of two gRNAs targeting the sense and antisense strand coupled to *Sp*Cas9-nickase; and (3) (single) gRNA/*Sp*Cas9 rescue employing single gRNAs (Figure 1B).[22,23]

In this paper, we describe the results of the initial screening of 16 *in silico*-designed *Sp*Cas9 and *Sp*Cas9n strategies targeting the c.5197-557G>T variant by minigene splicing assay. Eight of them were subsequently validated in patient-derived CPCs, thus showing the successful rescue of a splice defect in *ABCA4* by three different CRISPR-*Sp*Cas9 approaches directly in patient-derived CPCs. Ultimately, our work paves the way for the investigation of CRISPR-Cas9 genome editing as a therapeutic tool to permanently correct DIVs in the *ABCA4* gene.

## RESULTS

### Design of dgRNAs/*Sp*Cas9-, dgRNAs/*Sp*Cas9n-, and gRNA/*Sp*Cas9-mediated approaches to rescue missplicing induced by the *ABCA4* c.5197-557G>T variant

The c.5197-557G>T DIV is located in intron 36 (intron size 3,727 bp). The 5′ end of the c.5197-557G>T-induced pseudoexon is located 750 bp upstream exon 37. For the establishment of the three editing approaches, 11 single gRNAs were designed by *in silico* prediction, considering their on-target and off-target scores (Table S1). Five of the designed gRNAs are located upstream of the DIV (gRNA1, gRNA7, gRNA9, gRNA10, and gRNA11), three downstream of the DIV (gRNA5, gRNA6, and gRNA8), and three overlapping with the DIV itself (gRNA2, gRNA3, and gRNA4) (Figure 1C). The ability of the selected gRNAs to induce cleavage at the *ABCA4* genomic locus was preliminarily screened in HEK293T cells or patient-derived heterozygous *ABCA4* c.5197-557G>T fibroblasts (Table S1), depending on the overlap of the gRNA sequence to c.5197-557T.

The dgRNAs/*Sp*Cas9 approach aimed to delete a large segment of genomic DNA of ~600 bp encompassing the entire pseudoexon, while the dgRNAs/*Sp*Cas9n approach was designed to generate smaller deletions of 20–80 bp including the DIV site and part of the 3′ pseudoexon sequence induced by staggered nicks on the opposite strands.[23] Conversely, the gRNA/*Sp*Cas9 rescue approach employs a single gRNA targeted to sequences in close proximity to the DIV. Repair of the double-strand break (DSB) by the error-prone non-homologous end-joining (NHEJ) pathway eventually deletes the DIV site or alters adjacent sequences,[24,25] which is expected to reinstall correct splicing of the corresponding *ABCA4* transcript (Figure 1B).[26]

As for the dgRNAs/*Sp*Cas9 rescue approach, four different combinations of gRNAs (gRNAs 7 + 6, gRNAs 7 + 8, gRNAs 9 + 6, and gRNAs 9 + 8) were cloned in an *Sp*Cas9-2A-EGFP (2gRNA-PX458) backbone vector allowing the simultaneous expression of two gRNAs (2gRNA). To establish the dgRNAs/*Sp*Cas9n approach, a total of six gRNA combinations (gRNAs 10 + 5, gRNAs 4 + 5, gRNAs 10 + 6, gRNAs 4 + 6, gRNAs 11 + 5, and gRNAs 11 + 6) were cloned in a 2gRNA vector expressing *Sp*Cas9n-2A-EGFP (2gRNA-PX461).

For the gRNA/*Sp*Cas9 rescue, six gRNAs (gRNA1, gRNA2, gRNA3, gRNA4, gRNA5, and gRNA6) targeting sites in a region from −24 nt to +37 nt surrounding the DIV were selected and individually cloned in a vector expressing *Sp*Cas9-2A-EGFP (PX458) (Figure 1C).

### dgRNAs/*Sp*Cas9-, dgRNAs/*Sp*Cas9n-, and gRNA/*Sp*Cas9-mediated splicing rescue using an *ABCA4* c.5197-557G>T minigene model

To study the effect and potency of the three editing approaches in rescuing aberrant splicing induced by the *ABCA4* c.5197-557G>T DIV, minigene constructs encompassing *ABCA4* exon 36 and 37, referred to as c.5197-557G>T minigene (mutated) and WT minigene

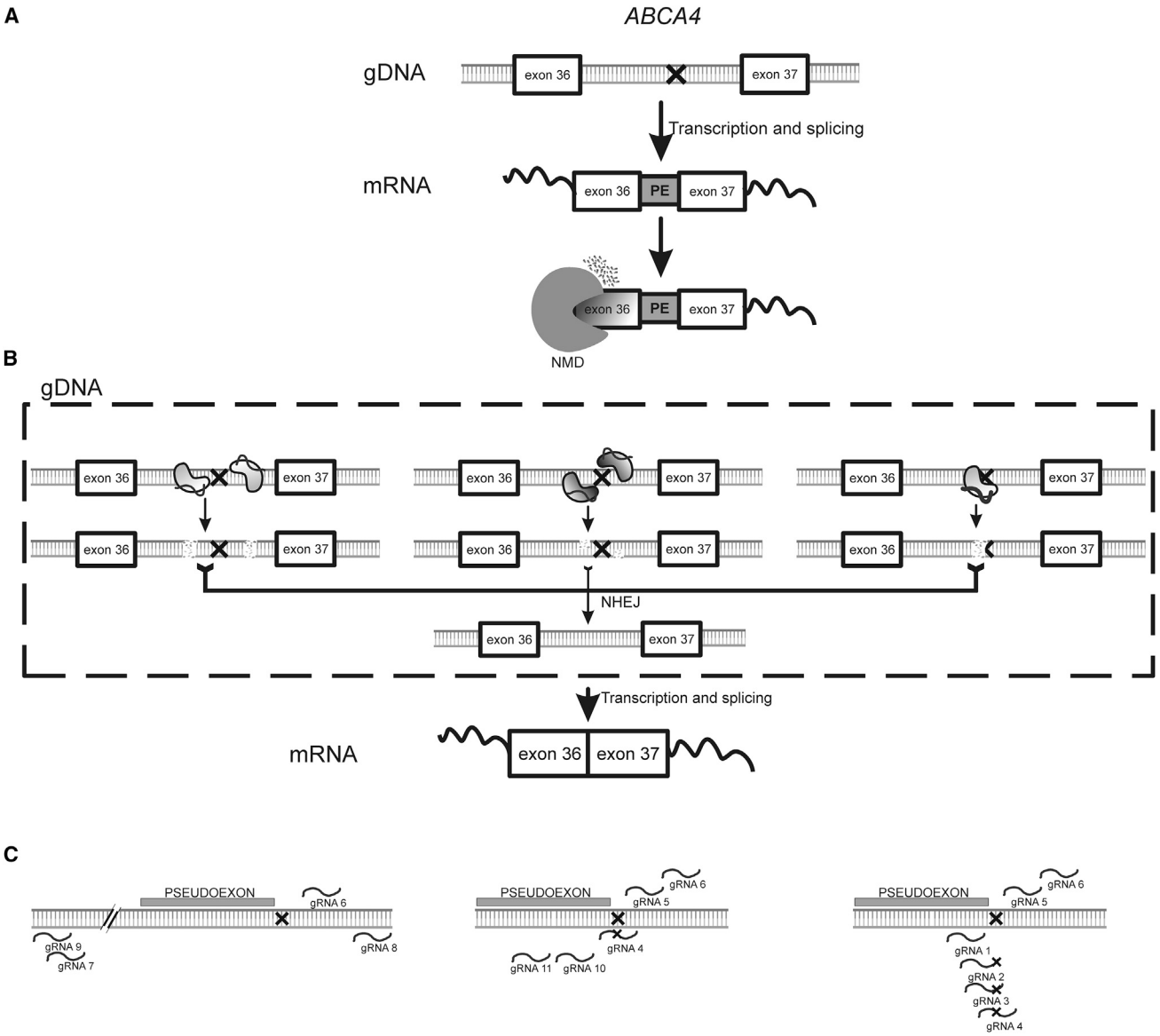


**Figure 1. Schematic representation of the design of the three *Sp*Cas9- and *Sp*Cas9n-mediated approaches to rescue the *ABCA4* c.5197-557G>T deep intronic variant**

(A) Splicing defect mechanism mediated by c.5197-557G>T DIV. Upon transcription and splicing, a 188-bp intronic sequence (pseudoexon [PE]) is retained in the mature mRNA transcript of *ABCA4*. The insertion of the PE creates a frameshift within the open reading frame leading to premature termination codon formation, which induces degradation of the transcript by nonsense-mediated mRNA decay (NMD). (B) Illustration of the three *Sp*Cas9- and *Sp*Cas9n-mediated approaches designed to rescue the *ABCA4* c.5197-557G>T DIV. *Sp*Cas9 is depicted in light gray and *Sp*Cas9n (nickase) in dark gray. (C) Location of the gRNAs with respect to the *ABCA4* c.5197-557G>T DIV and PE used in the three different approaches (from left to right): d(ual) gRNA/*Sp*Cas9 inducing double-strand breaks (DSB) up- and downstream of the PE for the generation of a large deletion of intronic sequences encompassing the entire PE, dgRNAs/*Sp*Cas9n inducing single strand breaks in close vicinity on opposite strands for the generation of small deletions encompassing parts of the PE, and single gRNA/*Sp*Cas9 inducing a DSB and non-homologous end-joining (NHEJ)-mediated indels in the vicinity of the deep intronic variant.

(wild type), were generated and used in co-transfection experiments in HEK293T cells. For validation of the minigenes, HEK293T were transfected with either the mutant or wild-type minigene, and the misspliced or correctly spliced transcripts were assessed by RT-PCR and analyzed by sequencing analysis. The resulting splicing patterns and identified transcripts are consistent with published data (Figure S1).[21]

In control HEKT293T cells co-transfected with the mutant minigene and a mock Cas9 targeted to a protospacer not present in GRCh38,

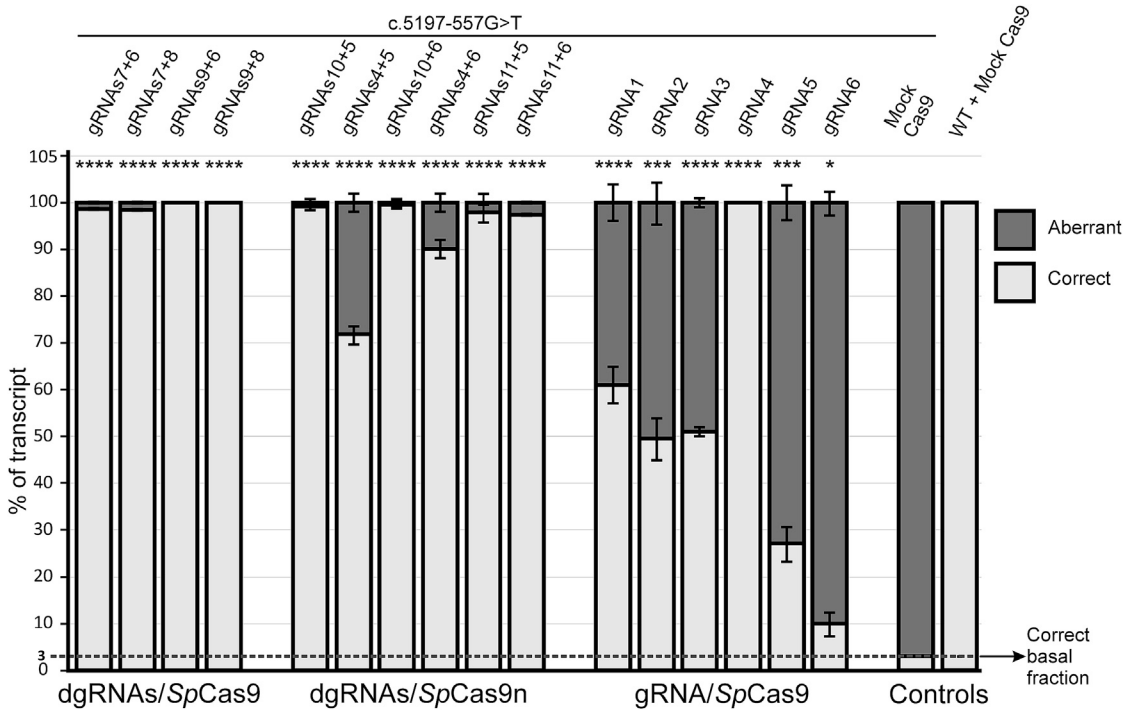


**Figure 2. Minigene splicing assay to evaluate the rescue of *ABCA4* c.5197-557G>T-induced splice defects in HEK293T**

HEK293T cells were co-transfected with wild-type (WT) or mutant (*ABCA4* c.5197-557G>T) *ABCA4* minigene constructs and plasmids encoding for the different (d)gRNA(s)/*Sp*Cas9 or dgRNAs/*Sp*Cas9n strategies. Relative proportions (percentage) of correctly and aberrantly spliced transcripts as quantified from RT-PCR products. A plasmid expressing *Sp*Cas9 and a scrambled gRNA was used as a Mock Cas9 control. Results are presented as mean ± SD (n = 2–3 independent transfections). Statistically significant changes in *ABCA4*% of correctly spliced transcript are expressed as *p ≤ 0.05, ***p ≤ 0.001, and ****p ≤ 0.0001 compared with Mock Cas9.

97.3% ± 0.1% aberrant and 2.7% ± 0.1% correct *ABCA4* minigene transcripts were detected. Of note, when the same primer pair was tested for endogenously expressed *ABCA4* transcript in HEK293T, no transcript was detected (data not shown). Expression of the four different dgRNAs/*Sp*Cas9 combinations increased the fraction of correctly spliced transcripts to 98.4% ± 0.1–100.0% ± 0.0. Similarly, an increase in the range of 71.9% ± 1.8% and 99.5% ± 0.7% of correctly spliced transcripts was observed for the six dgRNAs/*Sp*Cas9n combinations. When evaluating the six different gRNA/*Sp*Cas9 combinations, the fraction of correct transcript strongly varied depending on the gRNA used. With gRNA4 a complete rescue (100.0% ± 0.0%) was obtained, whereas intermediate rescue levels (from 51.1% ± 1.1% to 60.9% ± 4.0% correctly spliced transcripts) were observed with gRNA1, gRNA2, or gRNA3, and only minor rescue levels of 27.1% ± 3.6% and 10.0% ± 2.6% correctly spliced transcripts with gRNA5 and gRNA6, respectively (Figure 2 and Table S3).

### Transfection of patient-derived heterozygous *ABCA4* c.5197-557G>T cone photoreceptor precursor cells

To validate the CRISPR-*Sp*Cas9 strategies on the rescue of endogenously expressed *ABCA4* in an appropriate cellular model carrying the DIV, CPCs were differentiated from a human induced pluripotent stem cell (iPSC) line heterozygous for *ABCA4* DIV c.5197-557G>T (Figure S1). To verify successful differentiation of CPCs, qRT-PCR confirming the expression of the retinal marker genes *PAX6*, *RCVRN*, *OPN1SW*, *OPN1LW*, *RPE65*, *ABCA4*, and *POU5F1* (*OCT3/4*) was performed, comparing undifferentiated (day 0) and 30-day differentiated CPCs. Thirty-day-differentiated CPCs showed upregulation of *PAX6* (12- ± 8-fold), *RCVRN* (12- ± 5-fold), *RPE65* (213- ± 53-fold), *ABCA4* (21- ± 13-fold), and *OPN1SW* (2- ± 1-fold), and downregulation of *OPN1LW* (0.6- ± 0.1-fold) and *OCT3/4* (0.0005- ± 0.0002-fold) Figure S2.

Although patient-derived CPCs have been widely used to assess the efficacy of AON-mediated splicing modulation, to date no protocol for successful transfection or transduction of plasmids in CPCs has been described.[12,13,16,27] We have evaluated a number of commercial transfection reagents (e.g., Lipofectamine 3000 and Lipofectamine Stem Transfection Reagent, Thermo Fisher Scientific) as well as lentiviral particles for their efficiency to deliver the editing plasmids into CPCs. Virtually no transfected cells (as assessed by fluorescence microscopy) were seen using lipofection reagents, and only a low level of transduced cells was observed by transduction with a custom-made lentiviral vector batch (Figure S3A). We therefore established a reliable highly efficient electroporation protocol for the transfection of 30-day differentiated CPCs (Figure 3). Reproducible and consistent high transfection efficiencies of CPCs were achieved (average transfection efficiency: 79% ± 10% transfected cells in 30 independent

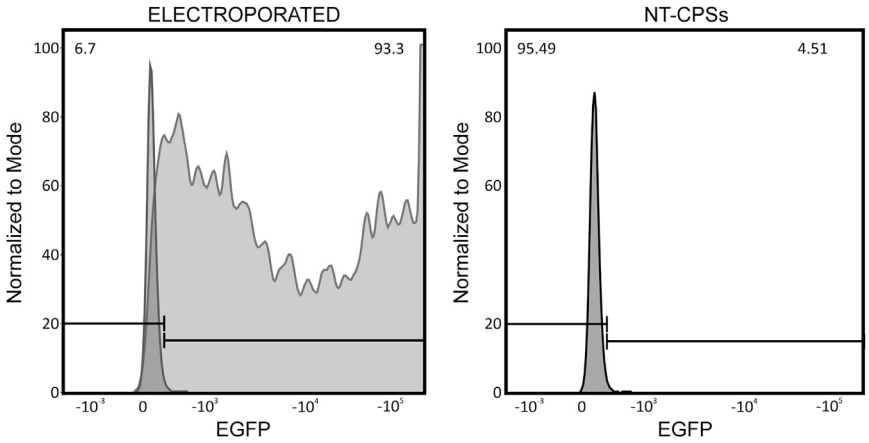


**Figure 3. Fluorescence-activated cell analysis of electroporated patient-derived heterozygous *ABCA4* c.5197-557 G>T cone photoreceptor precursor cells**

EGFP co-expressed with *Sp*Cas9 or *Sp*Cas9n from the employed editing constructs serves as marker for transfection efficacy. EGFP intensity was detected by flow cytometry (fluorescence-activated cell analysis). Transfection efficiency of representative electroporated cone photoreceptor precursor cells (CPCs) is shown (left panel). Non-transfected CPCs (NT-CPCs; right panel) were used as control to determine the background fluorescence and set the threshold for reliable identification of EGFP-expressing cells. In the top corner of each histogram (normalized to mode), the percentage of transfected cells (left panel) and non-transfected cells (right panel) in relation to the fluorescence intensity is shown.

electroporation rounds) (Figure S3B), and low levels of cell death were observed by comparing the number of electroporated cells with the number of attached cells 24 h post transfection. Specifically, an average of 80% ± 8% reattached cells were counted 24 h post transfection (n = 3). This protocol was selected to deliver the genome-editing plasmids into CPCs.

### *Sp*Cas9- and *Sp*Cas9n-based approaches allow splicing rescue in patient-derived heterozygous *ABCA4* c.5197-557G>T cone photoreceptor precursor cells

The eight most effective *Sp*Cas9(n)-based strategies tested in the minigene assay in HEK293T cells were selected for further validation in CPCs. Specifically, two gRNA combinations each for dgRNAs/*Sp*Cas9 (gRNAs 7 + 8 and gRNAs 9 + 6), as well as for dgRNAs/*Sp*Cas9n (gRNAs 10 + 5 and gRNAs 10 + 6) approaches were chosen. Four single gRNAs were selected for the gRNA/*Sp*Cas9 (gRNA2, gRNA3, gRNA4, and gRNA5) approach. In non-transfected CPCs, only 5.8% ± 0.6% aberrant *ABCA4* transcripts could be detected due to degradation of aberrant transcripts by NMD. To overcome this issue, CPCs were treated with 0.1 mg/mL cycloheximide (CHX), a known NMD blocker, 16 h prior to harvesting.[28] Non-transfected CPCs (NT-CPCs) and CPCs transfected with mock Cas9 were used as controls. Following pilot experiments showing the highest genome-editing efficacy at 7 days post electroporation, day-30 CPCs were transfected and subcultured for 7 days post electroporation before quantification of splicing rescue of *ABCA4* transcripts and editing efficiency on genomic DNA (gDNA) level.

All tested combinations were able to improve correct splicing, albeit with variable degrees of efficiency (Figure 4 and Table S4). The basal fraction of the correct transcript in our heterozygous patient-derived *ABCA4* c.5197-557G>T NT-CPCs treated with CHX was 72.5% ± 1.5% and is not altered by the electroporation procedure or the expression of Cas9 as seen in Mock Cas9 controls (71.9% ± 2.2%). For the two dgRNAs/*Sp*Cas9 combinations 90.9% ± 2.2% (gRNAs7+8) and 91.1% ± 3.5% (gRNAs 9 + 6) correctly spliced transcripts were observed indicating a splicing rescue of 67.1% ± 7.8% and 67.7% ± 12.8%, respectively (see materials and methods). The dgRNAs/*Sp*Cas9n combinations also resulted in splicing rescue in CPCs, but yielded lower fractions of correctly spliced transcripts (gRNAs 10 + 5: 85.4% ± 3.6%; gRNAs 10 + 6: 87.9% ± 3.0%) compared with dgRNAs/*Sp*Cas9. The relative ratio of correctly spliced transcript upon treatment indicates a splicing rescue of 47.1% ± 13.0% and 56.1% ± 10.8%, respectively. The four gRNA/*Sp*Cas9 combinations also achieved substantial relative splicing correction, with gRNA4 being outstandingly effective as it increased the fraction of correct transcripts to 95.2% ± 1.4% (82.7% ± 5.0% splicing correction), showing the highest relative rescue among the eight tested strategies. The gRNA/*Sp*Cas9 approach with gRNA2, gRNA3, or gRNA5 yielded similar fractions of correct transcripts of 83.9% ± 2.0%, 84.5% ± 1.0%, and 82.5% ± 5.6%, respectively, corresponding to a splicing rescue of around 40%.

To exclude secondary detrimental effects of the applied editing approaches on *ABCA4* splicing, the same eight strategies were tested in CPCs derived from a healthy control. Agarose gel electrophoresis was used to visualize the RT-PCR amplified splicing products spanning exon 35 to exon 41 of *ABCA4*. With all tested approaches and strategies, one single band corresponding to the expected fragment size of 838 bp was evident. Sanger sequencing of the RT-PCR products confirmed the *ABCA4* transcripts to be correctly spliced (Figure S4).

Upon successful application of the editing approaches in CPCs, an increase in the overall *ABCA4* transcript amount, resulting from rescued ABCA4 transcripts, should be observed.

One strategy for each approach was selected (gRNAs 7 + 8 for dgRNAs/*Sp*Cas9, gRNAs 10 + 6 for dgRNAs/*Sp*Cas9n, and gRNA4 for gRNA/*Sp*Cas9), and the plasmids were transfected in day-30 heterozygous *ABCA4* c.5197-557G>T CPCs. The cells were subcultured for 35 additional days to allow full *ABCA4* transcript turnover and to clear transfected CPCs from the editing plasmids, which occurred in the range of 20–25 days post electroporation as determined by visual

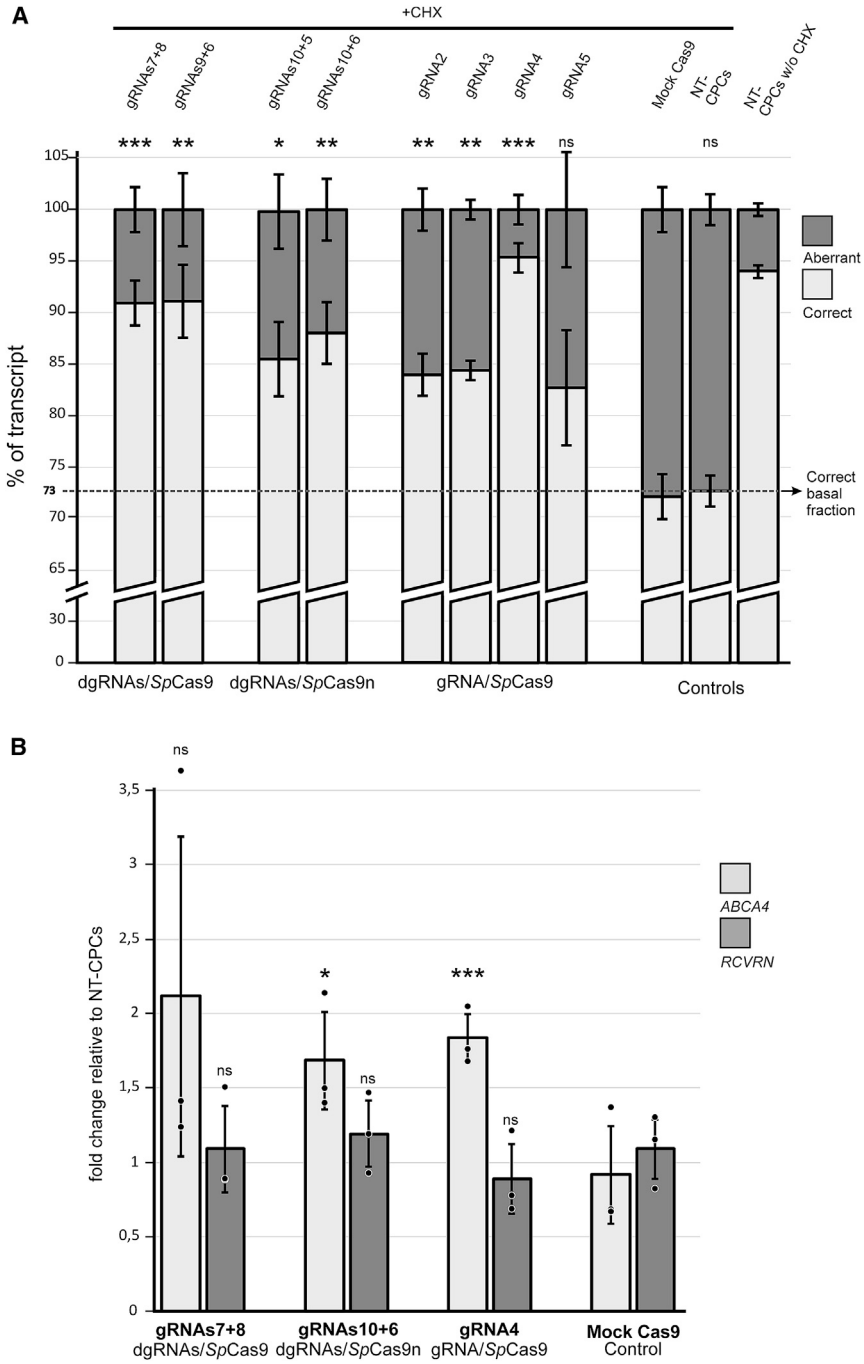


**Figure 4. Rescue of splice defects in patient-derived, heterozygous *ABCA4* c.5197-557G>T cone photoreceptor precursor cells**

(A) Electroporated cone photoreceptor precursor cells (CPCs) were analyzed 7 days post electroporation for assessment of relative rescue efficacy of the tested *Sp*Cas9- and *Sp*Cas9n-mediated approaches. Sixteen hours prior to harvesting, 0.1 mg/mL cycloheximide (CHX) was added. Non-transfected CPCs (NT-CPCs) without (w/o) CHX treatment, NT-CPCs treated with CHX, and cells transfected with Mock Cas9 (Cas9 + scramble gRNA) were used as controls. Relative quantification of aberrant and correct transcripts is shown. Results are presented as mean ± SD (n = 3). Statistically significant changes in *ABCA4*% of correctly spliced transcripts are expressed as *p ≤ 0.05, ***p ≤ 0.001, ****p ≤ 0.0001, and ns (not significant) compared with Mock Cas9. (B) qRT-PCR for *ABCA4* transcripts in patient-derived CPCs, heterozygous for *ABCA4* c.5197-557G>T at 35 days post electroporation. Relative quantification of total *ABCA4* and *RCVRN* transcripts is shown for one (d)gRNA(s)/*Sp*Cas9(n) combination per approach in CPCs without CHX treatment. Data are normalized to *GUSB* and expressed as fold change compared with NT-CPCs. Results are presented as mean ± SD including the data points of the three biological replicates. Statistically significant changes in *ABCA4* and *RCVRN* transcript levels are expressed as *p ≤ 0.05, ***p ≤ 0.001, and ns (not significant) compared with Mock Cas9.

control of EGFP-positive cells. Clearance of the editing plasmids was desired to prevent possible bias of qRT-PCR results due to sustained overexpression of an exogenous protein. Total mRNA was extracted from 65-day-old CPCs, and *ABCA4* and *RCVRN* transcript levels were quantified by qRT-PCR. For the gRNA4/*Sp*Cas9 combination, as well as the dgRNAs 10 + 6/*Sp*Cas9n combination, a significant 1.8- ± 0.2-fold and 1.7- ± 0.3-fold increase in *ABCA4* transcript levels compared with NT-CPCs was detected. For the dgRNAs 7 + 8/*Sp*Cas9 combination, a tendency toward increased *ABCA4* transcript levels was observed. Cone photoreceptor precursors transfected with Mock Cas9 showed a 0.9- ± 0.3-fold change in *ABCA4* transcript levels, comparable with NT-CPCs. In contrast, transcript levels of *RCVRN* did not change in the *Sp*Cas9- and *Sp*Cas9n-treated CPCs, confirming that increased transcript levels were specific for the target gene *ABCA4* (Figure 4B).

### gDNA editing profiles in patient-derived heterozygous *ABCA4* c.5197-557G>T cone photoreceptor precursor cells

To correlate the efficacy of the editing approaches to modify the genomic target site with the splicing rescue potential, the editing efficiency at the gDNA level was analyzed 7 days post electroporation in the CPCs. For the combinations used to evaluate increased expression of the overall *ABCA4* transcript amount (see above), gDNA editing efficiency was also assessed 35 days post electroporation. PCR fragment analysis on a Bioanalyzer 2100 instrument was used to determine editing efficacy (i.e., deletions of ~600 bp) for the dgRNAs/*Sp*Cas9 approaches, whereas for the dgRNAs/*Sp*Cas9n and gRNA/*Sp*Cas9 approaches high-throughput

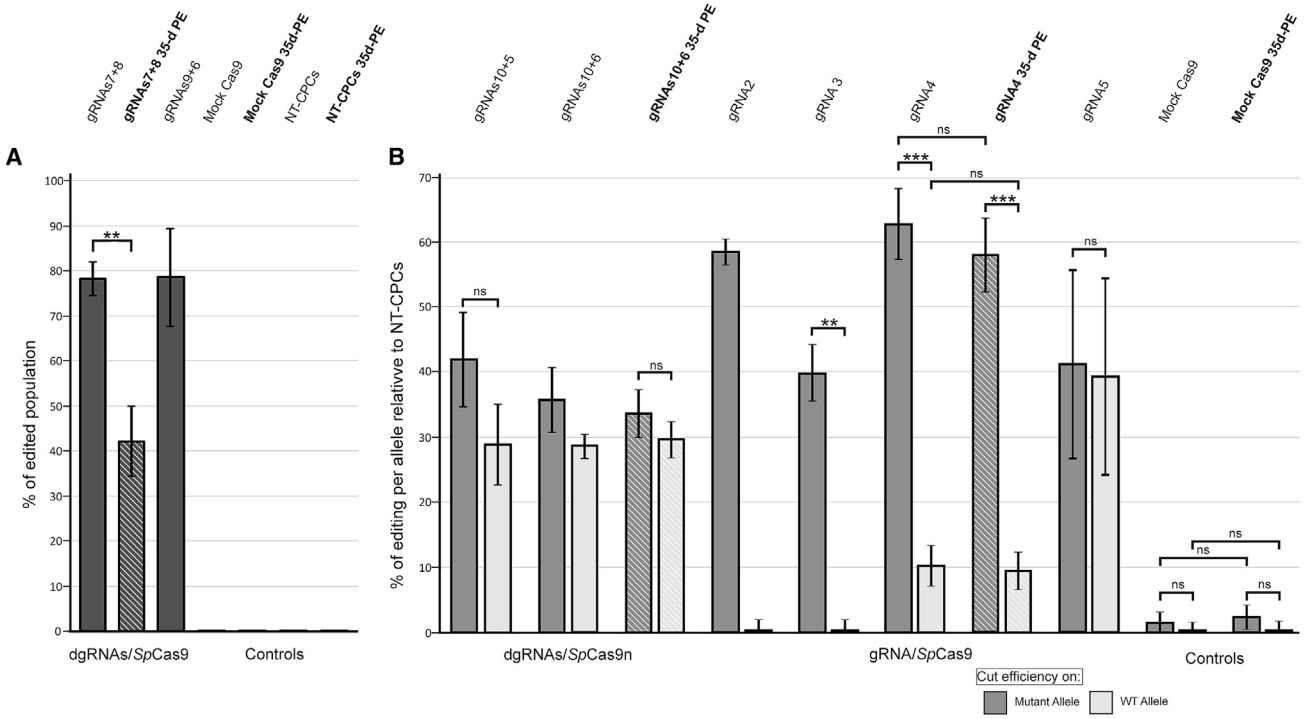


**Figure 5. gDNA editing efficiency of the *Sp*Cas9- and *Sp*Cas9n-mediated approaches in patient-derived heterozygous *ABCA4* c.5197-557G>T cone photoreceptor precursor cells**

(A) gDNA editing efficiency for the dgRNAs/*Sp*Cas9 approach calculated as percentage of edited alleles (not differentiating between wild-type and mutant alleles) at 7 days post electroporation. (B) dgRNAs/*Sp*Cas9n and gRNA/*Sp*Cas9 gDNA editing efficiencies 7 days post electroporation differentiated for editing of the mutant and wild-type allele and normalized to non-transfected cone photoreceptor precursor cells (NT-CPCs). For all samples, gRNAs10 + 6, gRNA4, Mock Cas9, and non-transfected control (NTC) gDNA editing efficiencies at 35 days post electroporation (35-d PE) are also shown (meshed shading). Results are presented as mean ± SD (n = 2–3). Statistically-significant differences between 7 days post electroporation and 35 days post electroporation as well as between mutant and wild-type (WT) alleles are expressed as $^{**}p \leq 0.01$, $^{***}p \leq 0.001$, and ns (not significant).

sequencing (HTS) was performed, since no discrete fragment size differences were expected. HTS analysis also allowed to determine differences in the editing efficacy of the c.5197-557G>T and wild-type allele (Figures 5A, 5B, and S5; Tables S5 and S6).

Using the dgRNAs/*Sp*Cas9 approach, gDNA editing efficiencies of 78.6% ± 8.8% and 78.2% ± 3.0% were achieved in CPCs at 7 days post electroporation for the gRNAs 9 + 6 and gRNAs 7 + 8, respectively. Notably, the percentage of edited cells dropped to 42.1% ± 6.4% at 35 days post electroporation in CPCs treated with dgRNAs 7 + 8/*Sp*Cas9 (Figure 5A), suggesting cellular senescence in CPCs treated with this strategy (see discussion). For the dgRNAs/*Sp*Cas9n approach, overall editing efficiencies of 34.4% ± 6.8% or 31.5% ± 3.6% were achieved in CPCs harvested 7 days post electroporation with editing constructs bearing gRNAs 10 + 5 and gRNAs 10 + 6, respectively. For dgRNAs 10 + 6/*Sp*Cas9n, editing efficiencies for both alleles were comparable (34.4% ± 2.2% mutant allele and 28.7% ± 5.0% wild-type allele), whereas the mutant allele was more efficiently edited compared with the wild-type allele when treating CPCs with dgRNAs 10 + 5/*Sp*Cas9n (40.2% ± 6.2% mutant allele and 28.7% ± 7.4% wild-type allele). The outcome of the dgRNAs/*Sp*Cas9n approach applying gRNAs 10 + 6 was also tested at 35 days post transfection. In this case, no difference could be seen on comparing efficacies at 7 days and 35 days post transfection (Figure 5B). For the gRNA/*Sp*Cas9 approach, gDNA editing efficiency of 58.5% ± 2.0%, 39.7% ± 5.9%, and 62.6% ± 3.1% were observed for the c.5197-57G>T allele with gRNA2, gRNA3, and gRNA4, respectively. As these three gRNAs overlap with the DIV, low cut efficiency was detected on the wild-type allele, implicating decent allelic preference of editing events. In contrast, gRNA5 does not overlap with the DIV and therefore, as expected, resulted in a similar gDNA editing efficiency at either allele (41.1% ± 15.0% on the mutant allele and 38.8% ± 14.5% on the wild-type allele). gDNA editing efficiency of the gRNA4/*Sp*Cas9 combination was also measured at 35 days post electroporation. Similarly to dgRNAs 7 + 8/*Sp*Cas9n, no significant difference was seen when compared with 7 days post transfection (Figure 5B).

## DISCUSSION

In this study, we investigated and proved effective various *Sp*Cas9 and *Sp*Cas9n approaches to rescue *ABCA4* missplicing caused by the DIV c.5197-557G>T using patient-derived CPCs as a cellular model. This

variant is a rare *ABCA4* disease-associated allele that has only been observed once in our local patient cohort and has never been observed in population databases (i.e., gnomAD browser). To our knowledge, a rescue of this DIV-induced splicing defect has only been shown by AONs in minigene assays but not on endogenously expressed *ABCA4* transcripts.[21] AON-mediated splicing correction acts at the transcriptional and splicing level, therefore not resulting in permanent correction of the genetic defect.[27,29] Although efficacy seems to be sustained for months, patients dosed with AON-based therapies necessitate recurrent intravitreal administrations, with risks of bleeding as well as cataract and intraocular infections.[30–33] Conversely, CRISPR-Cas9-mediated splicing correction would allow permanent correction at the genomic level, possibly by a single treatment.

We established a total of three different *Sp*Cas9 and *Sp*Cas9n approaches and evaluated their efficiency to correct *ABCA4* aberrant splicing by applying a minigene assay in HEK293T cells. All four chosen dgRNA combinations of the dgRNAs/*Sp*Cas9 approach achieved almost complete restoration of regular splicing at the *ABCA4* exon 36–37 junction of the minigene-derived transcripts (minimum: 98.4% ± 0.1%; maximum: 100.0% ± 0%), indicating that the deletion of part of intron 36, including the pseudoexon sequence, can effectively reverse aberrant splicing. The dgRNAs/*Sp*Cas9n approach also yielded substantial amounts of correctly spliced transcripts (minimum: 71.9% ± 1.8%; maximum: 97.9% ± 2.0%) and thus demonstrate that the deletion of part of the pseudoexon sequence, including the DIV, is able to rescue correct splicing. Single gRNA/*Sp*Cas9 induced DSBs also proved to be a practicable approach to target the DIV; however, considerable variability was observed with respect to the splicing rescue depending on the used gRNA. A general observation is that gRNA/*Sp*Cas9 targeting sites upstream of the DIV, in proximity of the strengthened cryptic donor splice site, results in a higher proportion of correct transcript (minimum: 49.6% ± 4.4%; maximum: 100.0% ± 0.0%) compared with target sites downstream of the DIV (minimum: 10.0% ± 2.6%; maximum: 27.1% ± 3.6%). This indicates that the mutational profiles (indels) that are able to rescue the splicing are more likely to be effective when introduced in close proximity to the DIV and the strengthened cryptic donor splice sites.

Although the use of a minigene splicing assay for preliminary screen of potential CRISPR-Cas9-based splicing rescue allows quick evaluation of strategies and screening for favorable single gRNAs or gRNA pairs,[17,34] the episomal nature of the plasmid and lack of any chromatin structure limits the minigene splicing assay to testing the effectiveness of introduced indels to correct splicing.[35] This means that the editing efficiency (intended as the ability to determine genomic breaks) of a given gRNA/Cas9 combination may substantially decrease when tested at the endogenous genomic locus, thereby affecting the overall efficacy on splicing rescue. Furthermore, it has been shown that euchromatin is targeted more efficiently by the CRISPR-Cas9 system than heterochromatin. Therefore, we comparatively evaluated the chosen editing strategies in *ABCA4*-expressing CPCs differentiated from a patient-derived iPSC cell line heterozygous for c.5197-557G>T. Although chromatin accessibility, and thereby genome-editing cleavage efficacy and outcomes, can differ *in vivo* compared with differentiated patient-derived cellular models,[36,37] the implementation of differentiated patient-derived cellular models (i.e., CPCs) for the assessment of CRISPR-Cas9-based therapies represents an important platform for evaluating editing dynamics of mutation-specific genome-editing approaches targeting rare alleles.[17]

To block NMD of the mutant *ABCA4* transcript in CPCs, CHX was applied and 27.5% ± 1.5% aberrant *ABCA4* transcript was detected in NT-CPCs. All three approaches and tested CRISPR-Cas9 compounds were able to reduce the fraction of aberrantly spliced transcripts and showed rescue potential consistent with the minigene splicing assay results, highlighting the value of this assay for the preliminary validation of genome-editing strategies.

In addition, we also demonstrated that for two of the three combinations (gRNAs 10 + 6/*Sp*Cas9 and gRNA4/*Sp*Cas9) tested in the long-term experiment, the absolute amount of *ABCA4* transcript significantly increased by 1.8- ± 0.2-fold and 1.7- ± 0.3-fold, indicating that the treatment also resulted in a lasting increase in *ABCA4* transcript levels when expression of the editing compounds faded out (Figure 4B).

Although splicing rescue in patient-derived CPCs was demonstrated, we wanted to further elucidate the relationship between gDNA editing efficacy and indel profiles with pre-mRNA splicing rescue potential. Although the use of two different protocols (fragment analysis for the dgRNAs/*Sp*Cas9 approach and HTS for the single gRNA/*Sp*Cas9 and dgRNAs/*Sp*Cas9n approaches) preclude a direct comparison, our results suggest that the gDNA editing efficiency, as calculated by fragment analysis for the dgRNAs/*Sp*Cas9 approach, translated into similar rescue potential (gRNAs 7 + 8: 78.2% ± 3.0% gDNA editing and 67.1% ± 7.8% splicing rescue; gRNAs 9 + 6: 78.6% ± 8.8% gDNA editing and 67.7% ± 12.8% splicing rescue). Similarly, the correlation between gDNA editing and the relative amount of rescued mRNA transcript was linear for gRNAs 10 + 5 but not for gRNAs 10 + 6 used in the dgRNAs/*Sp*Cas9n approach, as calculated by HTS. Specifically, for the dgRNAs 10 + 5/*Sp*Cas9n combination, 47.0% ± 13.0% splicing rescue was achieved with a gDNA editing efficiency of 40.2% ± 6.2%, whereas the dgRNAs 10 + 6/*Sp*Cas9n combination induced 56.1% ± 10.8% splicing rescue with a gDNA editing efficiency of only 34.4% ± 2.2% on the mutant allele. These findings may be attributed to mapping errors or larger deletions induced by the dgRNAs 10 + 6/*Sp*Cas9n that are beyond HTS detection. Furthermore, upon genome editing, stronger effects at the mRNA level compared with the level of gDNA editing outcomes has already been reported in the literature (Figures 4A, 5A, and 5B).[38,39] As for gRNA2, gRNA3, or gRNA4 used in the single gRNA/*Sp*Cas9 approach, it is interesting to note that a considerable fraction of the mutational profiles introduced at the targeted site do not result in the removal of the DIV. Nonetheless, the introduced indels are still

able to effectively perturb the strength of the pseudoexon cryptic splice site, resulting in a rescue of correct splicing (Figure S5). In the specific case of the most effective gRNA (gRNA4), around 30% of the generated indels result in a recurrent 1-bp deletion, converting the strong cryptic donor site sequence of the pseudoexon (5′-GTAAGT-3′) to a weaker one (5′-GTAGTA-3′).[40] Three of the four gRNAs used in the single gRNA/*Sp*Cas9 approach overlap with the *ABCA4* c.5197-557G>T variant, resulting in predominant editing of the mutant allele. Despite the use of the wild-type *Sp*Cas9, substantial specificity for the targeted mutant allele was obtained. In line with prior studies, application of gRNA4 showed the least discrimination between the mutant and the wild-type allele, as a mismatch at the 5′ end of gRNAs is more tolerated (Figure 1C).[41–43] Yet allele specificity is not mandatory for either of the evaluated strategies, since the editing of the wild-type allele did not interfere with correct splicing of the corresponding transcript (Figure S4).

The assessment of the gDNA editing 35 days post electroporation for dgRNAs 10 + 6/*Sp*Cas9n and gRNA4/*Sp*Cas9 revealed no difference compared with 7 days post electroporation, reflecting constant edited and unedited cell populations, also indicating that a plateau of effectiveness is achieved at 7 days post electroporation with non-replicating plasmid constructs. On the contrary, gRNAs 7 + 8 used in the dgRNAs/*Sp*Cas9 approach showed a substantial drop in gDNA editing efficiency and, hence, the number of edited cells at 35 days post electroporation (Figure 5A). Off-target-related genotoxicity of either gRNA7 or gRNA8 may be a tempting argument to explain this finding; however, CPCs analyzed 7 days post electroporation do not show signs of enhanced cell death (e.g., transfection efficiency comparable with the other strategies and high percentage of edited cell population). Considering that the expression of EGFP, and thereby *Sp*Cas9, is detected as soon as 20 h post electroporation, and that the cells repair Cas9-mediated DSBs with an average half-life of <10 h, genotoxicity resulting in cell death would be already evident at 7 days post electroporation.[44,45] Therefore, the drop in the percentage of edited population suggests to a greater extent that a fraction of the edited cell population entered cellular senescence due to response to DNA damage.[46] Of note, CPCs are considered immature cells and can still divide, albeit slowly. This finding may not be unexpected if considering that the dgRNAs/*Sp*Cas9 approach triggers four DSBs (two per allele)—in comparison with one DSB achieved by gRNA2, gRNA3, and gRNA4/*Sp*Cas9 strategies—and thus might be more potent in activating the TP53 pathway involved in regulating cell division in response to DNA damage.[46–50] The induction of *TP53* can hamper the growth of Cas9-edited cells and determine positive selective pressure for cells with pre-existing *TP53* mutations, thereby potentially inducing tumorigenesis.[51,52] Although postmitotic cells, like photoreceptors, are terminally differentiated and thus are non-dividing cells, the DNA damage and cellular stress induced by several DSBs may still lead to senescence, as has already been shown for postmitotic neurons.[53–55] Further studies are warranted to substantiate our findings and verify an increase in risk to induce damage in editing approaches based on multiple DSBs. In light of these arguments and the evidence, the implementation of approaches requiring a single gRNA/*Sp*Cas9 or not inducing DSBs (dgRNAs/*Sp*Cas9n) are advisable, especially when designed to only target the mutant allele. However, this may considerably reduce the number of suitable gRNAs and, therefore, the selection of specific and effective ones may be challenging or not possible. Furthermore, following the repair of DSBs by NHEJ, the introduction of indels may not be able to rescue the splicing and may considerably vary across different cell lines, hindering the scalability of such approaches.[26,56,57] On the other hand, protein engineering and directed evolution experiments can be undertaken to improve effectiveness and specificity of a given gRNA/*Sp*Cas9 strategy.

Off-target assessment was limited to scores based on mismatches to the gRNA sequence, showing substantial specificity of the used gRNAs (Table S1). Thorough off-target assessment, based on unbiased detection protocols (e.g., GUIDE-seq) was not planned, as it was beyond the scope and stage of this research. CPCs can be used to assess editing dynamics directly in patient-derived cell lines, thus providing a valuable platform accounting for genetic variability of different patients. However, to optimally assess potential off-target editing, the delivery of the CRISPR-Cas9 system should, as close as possible, mimic the methods and vehicle chosen for *in vivo* treatment, otherwise the number and sites of off-targets may be overestimated or non-translatable.[43,57–59] Since adeno-associated virus (AAV) delivery is currently the method of choice for delivering gene therapy in inherited retinal diseases, a more appropriate off-target evaluation should include AAV transduction of a given *Sp*Cas9(n) approach in patient-derived cellular models. The size of our current (d)gRNA(s)/*Sp*Cas9(n) combinations exceeds the AAV cargo capacity; therefore, single AAV delivery would not be possible. However, intein-based *trans*-splicing systems could be used to deliver our approaches via two different AAV particles.[60] Moreover, a class of small and efficient synthetic RNA-guided nucleases (sRGNs), deliverable via single AAV particles, have been recently described.[61] These sRGNs recognize similar protospacer adjacent motif sequences to *Sp*Cas9 (NNGG and NGG, respectively), resulting in target sites shifted by one nucleotide. As the mutational profiles generated upon Cas9-mediated DSBs do not depend on the enzyme used but on the cellular repair mechanisms,[26] we can speculate that adapting gRNA4 for coupling with the sRGNs would result in similar mutational profiles and, thus, splicing rescue. The implementation of sRGNs would translate to the possibility to advance our research toward preclinical investigation with the aim of validating approaches that are applicable *in vivo*.

In conclusion, effective rescue of aberrant splicing caused by a DIV in *ABCA4* was achieved by applying and comparing three different CRISPR-Cas9 approaches side by side in patient-derived CPCs, highlighting the potential of CRISPR-Cas9-mediated genome editing in rescuing disease-causing DIVs in *ABCA4*.

All eight strategies selected by minigene assay were shown to be effective in rescuing c.5197-557G>T variant missplicing in patient-derived CPCs, highlighting minigene assays as a valid platform for preliminary screening. The three CRSPR-Cas9 editing approaches evaluated

herein were shown to be applicable to rescue of the splicing defect induced by the c.5197-557G>T variant, and are therefore potentially transferable to other *ABCA4* DIVs. Finally, the highest efficiency was observed for the gRNA4/*Sp*Cas9 combination, which additionally is predicted to have no off-target sites (with up to two mismatches assessed by Cas-OFFinder) and showed strong preference to edit the mutant allele, a positive feature not determining the deletion of large genomic fragment, reducing the chance of chromosomal aberrations, conceivably limiting *TP53* activation, and therefore presenting encouraging hallmarks for scaling up.

## MATERIALS AND METHODS

### *In silico* gRNA and cloning design

Single guide RNAs and cloning experiments were designed on Benchling, a freely accessible online tool available at Benchling.com. The number of potential off-target sites were identified on Cas-OFFinder (http://www.rgenome.net/cas-offinder/).

### Plasmids

The wild-type minigene (pcDNA3.1/Zeo(+)WT-ABCA4Ex36-37-FLAG-T2A-mCherry) was generated by PCR amplification of the target *ABCA4* region using gDNA of a human control as template. A T2A-mCherry gBlock gene fragment was synthesized at Integrated DNA Technologies (München, Germany) and cloned downstream of the *ABCA4* fragments to visualize expression. Both fragments were cloned by three-fragment cloning into *Eco*RI-digested pcDNA3.1/Zeo(+) by Infusion cloning (NEBuilder HiFi DNA Assembly; New England Biolabs, Frankfurt am Main, Germany). The mutated c.5197-557G>T minigene construct (pcDNA3.1/Zeo(+) c.5197-557G>T-ABCA4Ex36-37-FLAG-T2A-mCherry) was obtained by site-directed mutagenesis of wild-type plasmid by *Pfu*Ultra High-Fidelity DNA Polymerase (Agilent Technologies, Waldbronn, Germany). Primers and gBlock sequences are listed in Table S2. The minigene plasmids include exons 36 and 37, and intron 36.

The fragment mU6-hU6 (2gRNA cassette) was obtained by Q5 High-Fidelity DNA Polymerase amplification (New England Biolabs) of pKLV2.2-mU6gRNA5(SapI)-hU6gRNA5(BbsI)-PGKpuroBFP-W (Addgene #133128) and cloned into PX458 (Addgene #48138) and PX461 (Addgene #48140), after removal of the hU6 cassette by *Afl*III and *Xba*I (New England Biolabs) digestion. The resulting plasmids are named 2gRNA-PX458 (mU6-hU6-*Sp*Cas9-2A-EGFP) and 2gRNA-PX461 (mU6-hU6-*Sp*Cas9n-2A-EGFP). Primers are listed in Table S2.

Lentiviral transfer plasmids pKLV2.2-CAG-*Sp*Cas9-2A-EGFP were obtained by first subcloning the CAG fragment and then inserting the *Sp*Cas9-2A-EGFP fragment. The CAG fragment was obtained by digesting PX458 with *Kpn*I and *Age*I (New England Biolabs) and subsequent treatment with DNA Polymerase I, Large (Klenow) Fragment (New England Biolabs) to generate blunt ends. The CAG fragment was then inserted by T4 DNA ligase in pKLV2.2 obtained by digestion with *ApaI* and *Not*I (New England Biolabs) and subsequent treatment with Klenow fragment to generate blunt ends. The resulting pKLV2.2-CAG plasmid was digested with *Blp*I (New England Biolabs). The *Sp*Cas9-2A-EGFP fragment was obtained by Q5 High-Fidelity DNA Polymerase amplification of PX458 and cloned into *Blp*I-digested pKLV2.2-CAG by Gibson assembly.

Lentiviral transfer plasmids pKLV2.2-PGK-*Sp*Cas9-2A-EGFP were obtained by first cloning the *Sp*Cas9-2A-EGFP fragment, amplified from PX458, into pKLV2.2-mU6gRNA5(SapI)-hU6gRNA5(BbsI)-PGKpuroBFP-W digested by *Xho*I and *Not*I. The fragment was cloned by Gibson assembly. The resulting pKLV2.2-2gRNA-PGK-*Sp*Cas9-2A-EGFP was then digested by *Apa*I and *Bam*HI (Thermo Fisher Scientific, Sindelfingen, Germany) to delete the 2gRNA cassette. Primers are listed in Table S2.

gRNAs were cloned into PX458 and PX461 using the *Bbs*I restriction site for the insertion of annealed synthetic oligonucleotides as described in the Zhang Lab General Cloning Protocol.[23] gRNA pairs were cloned into 2gRNA-PX458 and 2gRNA-PX461, using *Bbs*I and *SapI* (New England Biolabs) restriction sites (cloning protocol available on request). gRNAs are listed in Table S2.

Plasmid sequences are described in Table S7.

### Sanger sequencing

For sequencing PCR amplification products resulting in multiple bands, the PCR products were cloned by TA cloning (TA Cloning Kit; Thermo Fisher Scientific) following the manufacturer's protocol. Plasmid constructs were verified by Sanger sequencing using the sequencing primers listed in Table S2. Plasmids were extracted from bacterial cultures using silica-based purification columns (Monarch Plasmid Miniprep Kit; New England Biolabs) and sequenced using the BigDye Terminator v.1.1 kit (Thermo Fisher Scientific) according to the manufacturer's protocol. The same sequencing protocol was used to verify the success of gRNA cloning in the different backbone vectors. Sequencing of PCR amplicons resulting in a single band was carried out using the BigDye Terminator v.1.1 kit according to the manufacturer's protocol. Sequencing reactions were resolved on an ABI PRISM 3130xl Genetic Analyzer.

### Cell lines and culture conditions

HEK293T cells (ATCC, 293T/17) were cultured in Dulbecco's modified Eagle's medium (DMEM; Thermo Fisher Scientific, #41966029) supplemented with 10% fetal bovine serum (FBS; Thermo Fisher Scientific, #10270106), 10 U/mL penicillin/streptomycin (PenStrep; Thermo Fisher Scientific, #15140122) at 37°C in a 5% $CO_2$ humidified atmosphere.

A skin biopsy of the unaffected father of an STGD1 patient child (*ABCA4* c.[5197-557G>T]; [5917delG]), heterozygous for the DIV *ABCA4* c.5197-557G>T, was obtained upon informed written consent complying with the guidelines and approved by the local ethics committee (Project no. 124/2015BO1). Patient-derived fibroblast (Het-c.5197-557G>T) cells were expanded. Het-c.5197-557G>T

fibroblasts were cultured in DMEM supplemented with 10% FBS and 10 U/mL PenStrep at 37°C in a 5% $CO_2$ humidified atmosphere.

Reprogramming was done at the Stem Cell Technology Center, Radboud University Medical Center, the Netherlands, as a commercial service. The Het-c.5197-557G>T patient-derived fibroblasts were reprogrammed into iPSCs by a CytoTune-iPS 2.0 Sendai Reprogramming Kit (Thermo Fisher Scientific) and cultured in complete Essential E8 medium supplemented with 10 U/mL PenStrep at 37°C in a 5% $CO_2$ humidified atmosphere. As part of the reprogramming service, iPSCs were characterized for pluripotency markers by quantitative reverse transcription PCR (qRT-PCR) and immunocytochemistry, differentiation potential was evaluated by trilineage differentiation, and the karyotype was confirmed. Matrigel growth factor reduced basement membrane matrix (1:100) was used for coating (Corning, Kaiserslautern, Germany). A control iPSC line derived from a healthy proband was provided by Prof. Ludger Schöls and Dr. Stefan Hauser (DZNE, Tübingen, Germany). The Het-c.5197-557G>T patient-derived iPSCs and a control iPSC line underwent a 30-day differentiation protocol into CPCs, as described by Flamier and co-workers.[62] In brief, iPSC clumps were digested with Accutase (Sigma-Aldrich, Taufkirchen, Germany) and plated in a 12-well plate. Upon reaching 80% confluence, Essential E8 medium was changed into a differentiation medium consisting of DMEM/F12 (Thermo Fisher Scientific), supplemented with non-essential amino acids (Thermo Fisher Scientific), B27 supplements (Thermo Fisher Scientific), N2 supplements (Thermo Fisher Scientific), 10 ng/L insulin-like growth factor-1 (Sigma-Aldrich), 25 ng/L recombinant basic fibroblast growth factor (Sigma-Aldrich), 1 μg/L heparin (Sigma-Aldrich), 30 μg/L human recombinant COCO (Bio-Techne, Abingdon, Germany), and 0.5 mL/L Primocin (InvivoGen, Toulouse, France). The medium was changed every day for 30 days.

#### Transfection and lentiviral transduction of cell lines

HEK293T cells were seeded in a 24-well plate (250,000 cells/well) in DMEM without PenStrep and grown overnight. Cells were transfected using Lipofectamine 3000 (Thermo Fisher Scientific) with 500 ng of total plasmids (copy ratio for minigene assay 1:10—minigene:(d)gRNA/*Sp*Cas9(n) vector). Twenty-four hours after transfection the cell medium was changed, and cells were harvested 48 h post transfection for mRNA isolation.

Het-c.5197-557G>T fibroblasts were transfected by Neon electroporation according to the manufacturer's instructions (Thermo Fisher Scientific). In brief, cells were detached by Trypsin-EDTA (0.05%) (Thermo Fisher Scientific) (5 min at 37°C), harvested in 10 mL of DMEM and collected by centrifugation at 300 × *g* for 6 min. One million cells per reaction were resuspended in 100 μL of Buffer R, and 5 μg of endotoxin-free plasmid (editing plasmid: cells = ∼500,000:1) was used per electroporation reaction. Endotoxin-free plasmids were prepared using the EndoFree Plasmid Maxi Kit (QIAGEN, Hilden, Germany) following the manufacturer's protocol. Het-c.5197-557G>T fibroblasts were electroporated with the following settings: 1,400 V, 20 ms, 2 pulses. Electroporated cells were immediately plated in a well of a 6-well 1:50 plate with 2 mL of DMEM without PenStrep. Medium was replaced after 24 h with DMEM and 2 μg/mL puromycin (Thermo Fisher Scientific). The cells were treated with puromycin for 48 h prior to the extraction of gDNA for TIDE analysis.

Thirty-day old CPCs were transfected by Neon electroporation according to the manufacturer's instructions. In brief, CPCs were detached by Accutase treatment (5 min at 37°C), harvested in 10 mL of differentiation medium, and collected by centrifugation at 300 × *g* for 6 min. Two million cells per reaction were resuspended in 100 μL of Buffer R, and 20 μg of endotoxin-free plasmid (editing plasmid: cells = ∼1,000,000:1) was used per electroporation reaction. CPCs were electroporated with the following settings: 1,100 V, 30 ms, 2 pulses. Electroporated CPCs were immediately plated in a 1:50 Matrigel-coated well of a 6-well plate with 2 mL of differentiation medium without antibiotics and 10 nM ROCK inhibitors (Y-27632; Sigma-Aldrich). Medium was replaced after 24 h with differentiation medium. In both experiments, Mock Cas9 refers to basic PX458 (mock gRNA sequence: 5′-GGG TCT TCG AGA AGA CAC-3′ with no complementary sequence in the human genome).

Lentiviral particles were produced in HEK293T cells at 80% confluence in 10-cm plates transfected by Lipofectamine 3000 according to the manufacturer's protocol. A second-generation approach was used, employing pMD2.G (Addgene #12259), psPAX2 (Addgene #12260), and transfer vector pKLV2.2. The pKLV2.2 vector was obtained by removing the insert from pKLV2.2-mU6gRNA5(SapI)-hU6gRNA5(BbsI)-PGKpuroBFP-W. The medium was replaced 7 h post transfection (15 mL). The lentiviral supernatant was harvested at 24 h post transfection, the medium replaced, and harvested the second time at 52 h post transfection. The pooled lentiviral supernatant was filtered through a 0.45-μm pore size filter. Lentivirus particles were concentrated and purified by ultracentrifugation on a 20% sucrose cushion (%w/v). In brief, 8 mL of 20% sucrose was transferred to a 75-mL Ultra Bottle (Thermo Fisher Scientific), and lentiviral supernatant (30 mL) was gently added to the sucrose solution. The solution was centrifuged for 2 h at 80,000 × *g* and 4°C in a Sorvall WX Ultra 80+ centrifuge (Thermo Fisher Scientific). The supernatant was discharged and the lentiviral pellet resuspended in 300 μL of Opti-MEM (Thermo Fisher Scientific). Lentiviral particles were stored at −80°C.

An estimated amount of 2 million CPCs were transduced with 50 μL of the concentrated lentiviral vector preparation. The lentiviral vector was either directly added to CPCs in 1 mL of differentiation medium (for a well of a 12-well plate) or to CPCs which had been detached using Accutase (3 min at 37°C), resuspended in 1 mL of differentiation medium, and plated on a freshly coated well of a 12-well plate. Polybrene (Santa Cruz Biotechnology, Heidelberg, Germany) was added to enhance transduction at a final concentration of 8 μg/mL.

#### Tracking of indels by decomposition analysis

The preliminary screening of the cleavage potential of the gRNAs used in this study was performed through TIDE analysis, according

to the instructions present in the original publication.[63] Primers used for the amplification and sequencing of the genomic locus are listed in Table S2. Forward primers were used for sequencing.

### Flow cytometry

CPCs were dissociated into single cells by treatment with Accutase. Following harvesting, CPCs were rinsed once in phosphate-buffered saline (PBS; Sigma-Aldrich), filtered through a 100-μm cell strainer (pluriSelect, Leipzig, Germany), and resuspended in PBS at a concentration of about 500,000 cells/mL. Samples were analyzed on a BD FACS Canto II at the Flow Cytometry Core Facility—Berg of the Medical Faculty of the University of Tübingen. The cells were first analyzed for forward and side scattering, and then EGFP intensity was measured by 488 nm blue laser. FlowJo v10 was used for data analysis.

### Splicing analysis

Total RNA of HEK293T cells and CPCs was extracted using the peqGOLD Total RNA Kit (VWR Life Science, Bruchsal, Germany). One microgram of RNA was treated with 1 U of DNaseI (Sigma-Aldrich) following the manufacturer's instructions for 15 min at room temperature, followed by a 10-min heat inactivation step at 70°C after addition of 1 μL of stop buffer. DNaseI-treated RNA samples were used for cDNA synthesis applying the Maxima H Minus First Strand cDNA Synthesis Kit following the manufacturer's protocol (Thermo Fisher Scientific). Two microliters of the cDNA was used for PCR amplification employing Taq polymerase (Genaxxon Bioscience, Ulm, Germany). Primers are listed in Table S2. PCR products were purified using AMPure XP beads (Beckman Coulter, Krefeld, Germany) according to the manufacturer's protocol, and quantified on a Trinean DropSense 16 instrument (PerkinElmer LAS, Rodgau, Germany). Purified samples were analyzed on a 2100 Bioanalyzer instrument employing DNA 1000 Kit reagents (Agilent Technologies; Waldbronn, Germany) according to the manufacturer's protocol. Percentages of correctly spliced transcripts (CT) were calculated by the following formula: (CP/[CP + AP]) × 100, where CP is the molarity of the fragment corresponding to the correctly spliced RT-PCR product and AP is the molarity of the fragment corresponding to the aberrantly spliced RT-PCR product(s). For CPCs, percentage of rescue of mutant splicing was calculated by the following formula: (CT/CAT) × 100, where CAT is the percentage of aberrant transcripts in the NT-CPCs + CHX samples. Three biological replicates originating from three independent transfection/electroporations were performed for each strategy.

### Quantification of dual gRNAs/*Sp*Cas9-mediated gDNA cut efficiency

Genomic DNA was extracted using a peqGOLD Tissue DNA Mini Kit (VWR, Germany; #13339602) according to the manufacturer's protocol. Twenty-five nanograms of gDNA was used to amplify a fragment encompassing the dual target sites and some flanking sequences employing Taq polymerase. Primers are listed in Table S2. PCR products were purified using AMPure XP beads according to the manufacturer's protocol, and quantified on a Trinean DropSense 16 instrument. Purified samples were analyzed on a 2100 Bioanalyzer instrument employing DNA 1000 Kit reagents according to the manufacturer's protocol. Percentage of cut efficiency was calculated by the following formula: (ED/[WT + ED]) × 100, where ED is the molarity of the fragment(s) corresponding to the edited products and WT is the molarity of the fragment corresponding to the unedited product. Three independent biological replicates were performed.

### High-throughput library preparation for characterization of editing profiles

Genomic DNA was extracted using a peqGOLD Tissue DNA Mini Kit according to the manufacturer's protocol. A first PCR amplification (30 cycles) with 50 ng of gDNA was done using Q5 High-Fidelity DNA Polymerase (New England Biolabs) using hybrid primers with Nextera Read adapters attached the 5′ end. A second round of PCR amplification (35 cycles) was used to add dual indexes and the Illumina i5 and i7 adapters employing KAPA HiFi HotStart ReadyMix (Roche, Basel, Switzerland). Primers are listed in Table S2. PCR products were purified using AMPure XP beads according to the manufacturer's protocol. Quantification of the purified PCR products was done using AccuBlue NextGen dsDNA Quantitation Kit reagents (BIOTREND Chemikalien, Köln, Germany) and fluorescence measurement on a Spark microplate reader (Tecan Group, Männedorf, Switzerland). The quantified PCR products were pooled equimolarly to a final library concentration of 20 nmol/μL. The library was sequenced on a Miseq at the c.ATG/NGS Competence Center Tübingen core facility of the University Hospital Tübingen. Data analysis was performed on CRISRPesso2 (https://crispresso.pinellolab.partners.org/submission). The results are given as percentage of total reads normalized to the mean of the allele reads of NT-CPC samples. Negative values are not shown for logical reasons (Table S6).

### Gene expression quantification by qPCR

RNA isolation, DNaseI treatment, and reverse transcription into single-stranded cDNA were performed as described above. The cDNA reaction was diluted 1:5 with PCR-grade water, and 5 μL per reaction was used for qPCR. Each reaction was set up as follows in a 96-well plate (Biozym, Hessisch Oldendorf, Germany): 5 μL of 1:5-diluted cDNA, 10 μL of 2× QuantiTect SYBR Green PCR Master Mix (QIAGEN), 2 μL of forward primer (5 μM), 2 μL of reverse primer (5 μM), and 1 μL of PCR-grade water. Three technical replicates per condition were performed. Samples were run on a 7500 Real-Time PCR System (Applied Biosystems). Data evaluation was performed using the $2^{-\Delta\Delta Ct}$ method as described in Pfaffl.[64]

### Data analysis

qPCR statistical significance of biological replicates was performed on BootstRatio.[65] Unless specified otherwise, a two-tailed t test was used to assess differences in *ABCA4*% of correctly spliced transcript and gDNA cut efficiencies.

### Data availability

Targeted deep-sequencing data have been deposited at BioProject under the accession code PRJNA845890. All other relevant data

necessary for confirming the results reported in the paper are presented herein or are available from the authors upon reasonable request.

## SUPPLEMENTAL INFORMATION

Supplemental information can be found online at https://doi.org/10.1016/j.omtn.2022.07.023.

## ACKNOWLEDGMENTS

This research was funded by European Union's Horizon 2020—Marie Sklodowska-Curie Actions, grant number 813490 (to S.K.). The graphical abstract was created on BioRender.com.

## AUTHOR CONTRIBUTIONS

Conceptualization, P.D.A., B.W., and S.K.; methodology, investigation, and validation, P.D.A; supervision, P.R., B.W., and S.K.; resources, S.H., L.S., and K.S.; writing – original draft, P.D.A.; writing – review & editing, P.R., S.H., L.S., B.W., and S.K.

## DECLARATION OF INTERESTS

The authors declare no competing interests.

## REFERENCES

1. Tanna, P., Strauss, R.W., Fujinami, K., and Michaelides, M. (2017). Stargardt disease: clinical features, molecular genetics, animal models and therapeutic options. Br. J. Ophthalmol. *101*, 25–30.
2. Allikmets, R., Singh, N., Sun, H., Shroyer, N.F., Hutchinson, A., Chidambaram, A., Gerrard, B., Baird, L., Stauffer, D., Peiffer, A., et al. (1997). A photoreceptor cell-specific ATP-binding transporter gene (ABCR) is mutated in recessive Stargardt macular dystrophy. Nat. Genet. *15*, 236–246.
3. Cremers, F.P., van de Pol, D.J., van Driel, M., den Hollander, A.I., van Haren, F.J., Knoers, N.V., Tijmes, N., Bergen, A.A., Rohrschneider, K., Blankenagel, A., et al. (1998). Autosomal recessive retinitis pigmentosa and cone-rod dystrophy caused by splice site mutations in the Stargardt's disease gene ABCR. Hum. Mol. Genet. *7*, 355–362.
4. Koenekoop, R.K. (2003). The gene for Stargardt disease, ABCA4, is a major retinal gene: a mini-review. Ophthalmic genetic *24*, 75–80.
5. Shroyer, N.F., Lewis, R.A., Yatsenko, A.N., Wensel, T.G., and Lupski, J.R. (2001). Cosegregation and functional analysis of mutant ABCR (ABCA4) alleles in families that manifest both Stargardt disease and age-related macular degeneration. Hum. Mol. Genet. *10*, 2671–2678.
6. Yatsenko, A.N., Shroyer, N.F., Lewis, R.A., and Lupski, J.R. (2001). Late-onset Stargardt disease is associated with missense mutations that map outside known functional regions of ABCR (ABCA4). Hum. Genet. *108*, 346–355.
7. Zernant, J., Schubert, C., Im, K.M., Burke, T., Brown, C.M., Fishman, G.A., Tsang, S.H., Gouras, P., Dean, M., and Allikmets, R. (2011). Analysis of the ABCA4 gene by next-generation sequencing. Invest. Ophthalmol. Vis. Sci. *52*, 8479–8487.
8. Zernant, J., Lee, W., Collison, F.T., Fishman, G.A., Sergeev, Y.V., Schuerch, K., Sparrow, J.R., Tsang, S.H., and Allikmets, R. (2017). Frequent hypomorphic alleles account for a significant fraction of ABCA4 disease and distinguish it from age-related macular degeneration. J. Med. Genet. *54*, 404–412.
9. Braun, T.A., Mullins, R.F., Wagner, A.H., Andorf, J.L., Johnston, R.M., Bakall, B.B., Deluca, A.P., Fishman, G.A., Lam, B.L., Weleber, R.G., et al. (2013). Non-exomic and synonymous variants in ABCA4 are an important cause of Stargardt disease. Hum. Mol. Genet. *22*, 5136–5145.
10. Zernant, J., Xie, Y.A., Ayuso, C., Riveiro-Alvarez, R., Lopez-Martinez, M.A., Simonelli, F., Testa, F., Gorin, M.B., Strom, S.P., Bertelsen, M., et al. (2014). Analysis of the ABCA4 genomic locus in Stargardt disease. Hum. Mol. Genet. *23*, 6797–6806.
11. Sangermano, R., Khan, M., Cornelis, S.S., Richelle, V., Albert, S., Garanto, A., Elmelik, D., Qamar, R., Lugtenberg, D., van den Born, L.I., et al. (2018). *ABCA4* midigenes reveal the full splice spectrum of all reported noncanonical splice site variants in Stargardt disease. Genome Res. *28*, 100–110.
12. Albert, S., Garanto, A., Sangermano, R., Khan, M., Bax, N.M., Hoyng, C.B., Zernant, J., Lee, W., Allikmets, R., Collin, R.W.J., et al. (2018). Identification and rescue of splice defects caused by two neighboring deep-intronic ABCA4 mutations underlying Stargardt disease. Am. J. Hum. Genet. *102*, 517–527.
13. Khan, M., Arno, G., Fakin, A., Parfitt, D.A., Dhooge, P.P.A., Albert, S., Bax, N.M., Duijkers, L., Niblock, M., Hau, K.L., et al. (2020). Detailed phenotyping and therapeutic strategies for intronic ABCA4 variants in Stargardt disease. Mol. Ther. Nucleic Acids *21*, 412–427.
14. Zhang, Z., Xin, D., Wang, P., Zhou, L., Hu, L., Kong, X., and Hurst, L.D. (2009). Noisy splicing, more than expression regulation, explains why some exons are subject to nonsense-mediated mRNA decay. BMC Biol. *7*, 23.
15. Grieger, J.C., and Samulski, R.J. (2005). Packaging capacity of adeno-associated virus serotypes: impact of larger genomes on infectivity and postentry steps. J. Virol. *79*, 9933–9944.
16. Garanto, A., Duijkers, L., Tomkiewicz, T.Z., and Collin, R.W.J. (2019). Antisense oligonucleotide screening to optimize the rescue of the splicing defect caused by the recurrent deep-intronic *ABCA4* variant c.4539+2001G>A in Stargardt disease. Genes *10*, 452.
17. Maeder, M.L., Stefanidakis, M., Wilson, C.J., Baral, R., Barrera, L.A., Bounoutas, G.S., Bumcrot, D., Chao, H., Ciulla, D.M., DaSilva, J.A., et al. (2019). Development of a gene-editing approach to restore vision loss in Leber congenital amaurosis type 10. Nat. Med. *25*, 229–233.
18. Bansal, M., Acharya, S., Sharma, S., Phutela, R., Rauthan, R., Maiti, S., and Chakraborty, D. (2021). CRISPR Cas9 based genome editing in inherited retinal dystrophies. Ophthalmic Genet. *42*, 365–374.
19. Maule, G., Casini, A., Montagna, C., Ramalho, A.S., De Boeck, K., Debyser, Z., Carlon, M.S., Petris, G., and Cereseto, A. (2019). Allele specific repair of splicing mutations in cystic fibrosis through AsCas12a genome editing. Nat. Commun. *10*, 3556.
20. Vázquez-Domínguez, I., Garanto, A., and Collin, R.W.J. (2019). Molecular therapies for inherited retinal diseases-current standing, opportunities and challenges. Genes *10*, 654.
21. Bauwens, M., Garanto, A., Sangermano, R., Naessens, S., Weisschuh, N., De Zaeytijd, J., Khan, M., Sadler, F., Balikova, I., Van Cauwenbergh, C., et al. (2019). ABCA4-associated disease as a model for missing heritability in autosomal recessive disorders: novel noncoding splice, cis-regulatory, structural, and recurrent hypomorphic variants. Genet. Med. *21*, 1761–1771.
22. Doudna, J.A., and Charpentier, E. (2014). Genome editing. The new frontier of genome engineering with CRISPR-Cas9. Science *346*, 1258096.
23. Ran, F.A., Hsu, P.D., Wright, J., Agarwala, V., Scott, D.A., and Zhang, F. (2013). Genome engineering using the CRISPR-Cas9 system. Nat. Protoc. *8*, 2281–2308.
24. Chiruvella, K.K., Liang, Z., and Wilson, T.E. (2013). Repair of double-strand breaks by end joining. Cold Spring Harb. Perspect Biol. *5*, a012757.
25. Her, J., and Bunting, S.F. (2018). How cells ensure correct repair of DNA double-strand breaks. J. Biol. Chem. *293*, 10502–10511.
26. Allen, F., Crepaldi, L., Alsinet, C., Strong, A.J., Kleshchevnikov, V., De Angeli, P., Páleníková, P., Khodak, A., Kiselev, V., Kosicki, M., et al. (2018). Predicting the mutations generated by repair of Cas9-induced double-strand breaks. Nat. Biotechnol. https://doi.org/10.1038/nbt.4317.
27. Dulla, K., Slijkerman, R., van Diepen, H.C., Albert, S., Dona, M., Beumer, W., Turunen, J.J., Chan, H.L., Schulkens, I.A., Vorthoren, L., et al. (2021). Antisense oligonucleotide-based treatment of retinitis pigmentosa caused by USH2A exon 13 mutations. Mol. Ther. *29*, 2441–2455.
28. Durand, S., Cougot, N., Mahuteau-Betzer, F., Nguyen, C.H., Grierson, D.S., Bertrand, E., Tazi, J., and Lejeune, F. (2007). Inhibition of nonsense-mediated mRNA decay (NMD) by a new chemical molecule reveals the dynamic of NMD factors in P-bodies. J. Cell Biol. *178*, 1145–1160.
29. Lindholm, M.W., Elmén, J., Fisker, N., Hansen, H.F., Persson, R., Møller, M.R., Rosenbohm, C., Ørum, H., Straarup, E.M., and Koch, T. (2021). PCSK9 LNA

antisense oligonucleotides induce sustained reduction of LDL cholesterol in nonhuman primates. Mol. Ther. *20*, 376–381.

30. Cideciyan, A.V., Jacobson, S.G., Ho, A.C., Garafalo, A.V., Roman, A.J., Sumaroka, A., Krishnan, A.K., Swider, M., Schwartz, M.R., and Girach, A. (2021). Durable vision improvement after a single treatment with antisense oligonucleotide sepofarsen: a case report. Nat. Med. *27*, 785–789.
31. Cideciyan, A.V., Jacobson, S.G., Drack, A.V., Ho, A.C., Charng, J., Garafalo, A.V., Roman, A.J., Sumaroka, A., Han, I.C., Hochstedler, M.D., et al. (2018). Effect of an intravitreal antisense oligonucleotide on vision in Leber congenital amaurosis due to a photoreceptor cilium defect. Nat. Med. *25*, 225–228.
32. Shah, C.P., Garg, S.J., Vander, J.F., Brown, G.C., Kaiser, R.S., and Haller, J.A.; Post-Injection Endophthalmitis (PIE) Study Team (2011). Outcomes and risk factors associated with endophthalmitis after intravitreal injection of anti-vascular endothelial growth factor agents. Ophthalmology *118*, 2028–2034.
33. Hahn, P., Jiramongkolchai, K., Stinnett, S., Daluvoy, M., and Kim, T. (2016). Rate of intraoperative complications during cataract surgery following intravitreal injections. Eye *30*, 1101–1109.
34. Sanz, D.J., and Harrison, P.T. (2019). Minigene assay to evaluate CRISPR/Cas9-based excision of intronic mutations that cause aberrant splicing in human cells. Bio Protoc *9*, e3251.
35. Daer, R.M., Cutts, J.P., Brafman, D.A., and Haynes, K.A. (2016). The impact of chromatin dynamics on Cas9-mediated genome editing in human cells. ACS Synth. Biol. *6*, 428–438.
36. Daer, R.M., Cutts, J.P., Brafman, D.A., and Haynes, K.A. (2017). The impact of chromatin dynamics on Cas9-mediated genome editing in human cells. ACS Synth. Biol. *17*, 428–438.
37. Schep, R., Brinkman, E.K., Leemans, C., Vergara, X., van der Weide, R.H., Morris, B., van Schaik, T., Manzo, S.G., Peric-Hupkes, D., van den Berg, J., et al. (2021). Impact of chromatin context on Cas9-induced DNA double-strand break repair pathway balance. Mol. Cell. *81*, 2216–2230.e10.
38. Erwood, S., Laselva, O., Bily, T.M.I., Brewer, R.A., Rutherford, A.H., Bear, C.E., and Ivakine, E.A. (2020). Allele-specific prevention of nonsense-mediated decay in cystic fibrosis using homology-independent genome editing. Mol. Ther. Methods Clin. Dev. *17*, 1118–1128.
39. Jang, H., Jo, D.H., Cho, C.S., Shin, J.H., Seo, J.H., Yu, G., Gopalappa, R., Kim, D., Cho, S.R., Kim, J.H., et al. (2021). Application of prime editing to the correction of mutations and phenotypes in adult mice with liver and eye diseases. Nat. Biomed. Eng. https://doi.org/10.1038/s41551-021-00788-9.
40. Desmet, F.O., Hamroun, D., Lalande, M., Collod-Béroud, G., Claustres, M., and Béroud, C. (2009). Human Splicing Finder: an online bioinformatics tool to predict splicing signals. Nucleic Acids Res. *37*, e67.
41. Cong, L., Ran, F.A., Cox, D., Lin, S., Barretto, R., Habib, N., Hsu, P.D., Wu, X., Jiang, W., Marraffini, L.A., et al. (2013). Multiplex genome engineering using CRISPR/Cas systems. Science *339*, 819–823.
42. Jinek, M., Chylinski, K., Fonfara, I., Hauer, M., Doudna, J.A., and Charpentier, E. (2012). A programmable dual-RNA-guided DNA endonuclease in adaptive bacterial immunity. Science *337*, 816–821.
43. Hsu, P.D., Scott, D.A., Weinstein, J.A., Ran, F.A., Konermann, S., Agarwala, V., Li, Y., Fine, E.J., Wu, X., Shalem, O., et al. (2013). DNA targeting specificity of RNA-guided Cas9 nucleases. Nat. Biotechnol. *31*, 827–832.
44. Brinkman, E.K., Chen, T., de Haas, M., Holland, H.A., Akhtar, W., and van Steensel, B. (2018). Kinetics and fidelity of the repair of Cas9-induced double-strand DNA breaks. Mol. Cell. *70*, 801–813.e6.
45. Joung, J., Konermann, S., Gootenberg, J.S., Abudayyeh, O.O., Platt, R.J., Brigham, M.D., Sanjana, N.E., and Zhang, F. (2017). Genome-scale CRISPR-Cas9 knockout and transcriptional activation screening. Nat. Protoc. *12*, 828–863.
46. Hayflick, l. (1965). The limited in vitro lifetime of human diploid cell strains. Exp. Cell Res. *37*, 614–636.
47. Haapaniemi, E., Botla, S., Persson, J., Schmierer, B., and Taipale, J. (2018). CRISPR-Cas9 genome editing induces a p53-mediated DNA damage response. Nat. Med. *24*, 927–930.
48. Ihry, R.J., Worringer, K.A., Salick, M.R., Frias, E., Ho, D., Theriault, K., Kommineni, S., Chen, J., Sondey, M., Ye, C., et al. (2018). p53 inhibits CRISPR-Cas9 engineering in human pluripotent stem cells. Nat. Med. *24*, 939–946.
49. van den Berg, J., Manjón, A.G., Kielbassa, K., Feringa, F.M., Freire, R., and Medema, R.H. (2018). A limited number of double-strand DNA breaks is sufficient to delay cell cycle progression. Nucleic Acids Res. *46*, 10132–10144.
50. Enache, O.M., Rendo, V., Abdusamad, M., Lam, D., Davison, D., Pal, S., Currimjee, N., Hess, J., Pantel, S., Nag, A., et al. (2020). Cas9 activates the p53 pathway and selects for p53-inactivating mutations. Nat. Genet. *52*, 662–668.
51. Leibowitz, M.L., Papathanasiou, S., Doerfler, P.A., Blaine, L.J., Sun, L., Yao, Y., Zhang, C.Z., Weiss, M.J., and Pellman, D. (2021). Chromothripsis as an on-target consequence of CRISPR-Cas9 genome editing. Nat. Genet. *53*, 895–905.
52. Sinha, S., Barbosa, K., Cheng, K., Leiserson, M.D.M., Jain, P., Deshpande, A., Wilson, D.M., 3rd, Ryan, B.M., Luo, J., Ronai, Z.A., et al. (2021). A systematic genome-wide mapping of oncogenic mutation selection during CRISPR-Cas9 genome editing. Nat. Commun. *12*, 6512.
53. Jurk, D., Wang, C., Miwa, S., Maddick, M., Korolchuk, V., Tsolou, A., Gonos, E.S., Thrasivoulou, C., Saffrey, M.J., Cameron, K., et al. (2021). Postmitotic neurons develop a p21-dependent senescence-like phenotype driven by a DNA damage response. Aging Cell *11*, 996–1004.
54. Sedelnikova, O.A., Horikawa, I., Zimonjic, D.B., Popescu, N.C., Bonner, W.M., and Barrett, J.C. (2004). Senescing human cells and ageing mice accumulate DNA lesions with unrepairable double-strand breaks. Nat. Cell Biol. *6*, 168–170.
55. von Zglinicki, T., Wan, T., and Miwa, S. (2020). Senescence in post-mitotic cells: a driver of aging? Antioxid. Redox. Signal. *34*, 308–323.
56. Shen, M.W., Arbab, M., Hsu, J.Y., Worstell, D., Culbertson, S.J., Krabbe, O., Cassa, C.A., Liu, D.R., Gifford, D.K., and Sherwood, R.I. (2018). Predictable and precise template-free CRISPR editing of pathogenic variants. Nature *563*, 646–651.
57. Frock, R.L., Hu, J., Meyers, R.M., Ho, Y.J., Kii, E., and Alt, F.W. (2014). Genome-wide detection of DNA double-stranded breaks induced by engineered nucleases. Nat. Biotechnol. *33*, 179–186.
58. Gangopadhyay, S.A., Cox, K.J., Manna, D., Lim, D., Maji, B., Zhou, Q., and Choudhary, A. (2019). Precision control of CRISPR-Cas9 using small molecules and light. Biochemistry *58*, 234–244.
59. Chen, X., Chen, Y., Xin, H., Wan, T., and Ping, Y. (2020). Near-infrared optogenetic engineering of photothermal nanoCRISPR for programmable genome editing. Proc. Natl. Acad. Sci. USA *117*, 2395–2405.
60. Tornabene, P., Trapani, I., Minopoli, R., Centrulo, M., Lupo, M., de Simone, S., Tiberi, P., Dell'Aquila, F., Marrocco, E., Iodice, C., et al. (2019). Intein-mediated protein trans-splicing expands adeno-associated virus transfer capacity in the retina. Sci. Transl. Med. *11*, eaav4523.
61. Schmidt, M.J., Gupta, A., Bednarski, C., Gehrig-Giannini, S., Richter, F., Pitzler, C., Gamalinda, M., Galonska, C., Takeuchi, R., Wang, K., et al. (2021). Improved CRISPR genome editing using small highly active and specific engineered RNA-guided nucleases. Nat. Commun. *12*, 4219.
62. Flamier, A., Barabino, A., and Gilbert, B. (2016). Differentiation of human embryonic stem cells into cone photoreceptors. Bio Protoc *6*, e1870.
63. Brinkman, E.K., Amendola, M., and van Steensel, B. (2014). Easy quantitative assessment of genome editing by sequence trace decomposition. Nucleic Acids Res. *42*, e168.
64. Pfaffl, M.W. (2001). A new mathematical model for relative quantification in real-time RT–PCR. Nucleic Acids Res. *29*, e45.
65. Clèries, R., Galvez, J., Espino, M., Ribes, J., Nunes, V., and de Heredia, M.L. (2012). BootstRatio: a web-based statistical analysis of fold-change in qPCR and RT-qPCR data using resampling methods. Comput. Biol. Med. Apr. *42*, 438–445.